Noninvasively imaging pH at the surface of implanted orthopedic devices with X-ray excited luminescence chemical imaging (XELCI).

Unaiza Uzair , **Donald Benza** ,[†], **Caleb J. Behrend**[‡], **Jeffrey N. Anker**[*],

Department of Chemistry, Center for Optical Materials Science and Engineering (COMSET) and Environmental Toxicology Program, Clemson University, Clemson SC

[†]Department of Electrical and Computer Engineering, Clemson University, Clemson, SC

[‡]OrthoArizona, Phoenix AZ

Abstract

Implanted medical device-associated infections are a leading cause of fixation failure and early diagnosis is key to successful treatment. During infection, acidosis near the implant plays a role in antibiotic resistance and low pH is a potential infection indicator. Herein, we describe a pH sensor which attaches to implants to noninvasively image local pH with high spatial resolution. The sensor has two layers: a scintillator layer which emits 620 and 700 nm light upon X-ray irradiation, and a pH indicator layer containing bromocresol green dye that absorbs 620 nm luminescence in neutral/basic pH and passes 700 nm light at all pH. We also developed a dedicated imaging system capable of scanning relatively large specimens through thick tissue. A focused X-ray beam irradiates one spot on the sensor, and the 620 to 700 nm peak ratio is measured to determine local pH; images are acquired by scanning the X-ray beam across the surface and measuring pH point-by-point. The sensor was covered with varying thickness slices of chicken breast tissue (0-19 mm) to evaluate how tissue affects peak intensity and ratio. Thick tissue attenuated both 620 nm and 700 nm light, with more attenuation at 620 nm than 700 nm. Although this spectral distortion shifted the pH calibration curve, the effect could be corrected for using a scintillator film region with no pH-indicator layer as a spectral reference. The sensor was attached to an orthopedic plate affixed to a human cadaveric tibia and imaged through tissue. The approach provides both high spatial resolution from focused X-ray excitation, and surface chemical specificity from the indicator dye providing a tool for imaging local pH through tissue.
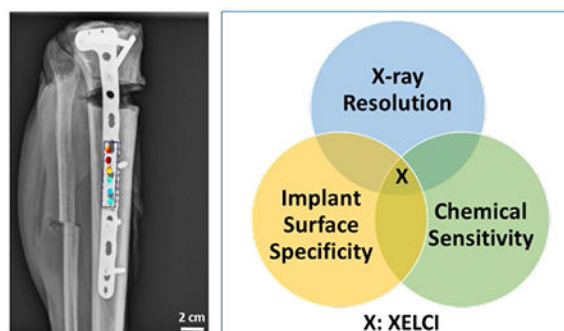
Graphical Abstract

[*]**Corresponding Author** janker@clemson.edu.
Author Contributions
All authors have given approval to the final version of the manuscript.

Authors are required to submit a graphic entry for the Table of Contents (TOC) that, in conjunction with the manuscript title, should give the reader a representative idea of one of the following: A key structure, reaction, equation, concept, or theorem, etc., that is discussed in the manuscript. Consult the journal's Instructions for Authors for TOC graphic specifications.

Keywords

pH sensing; pH imaging; XELCI; X-ray scintillation; tissue scattering; bioimaging

As the population ages, orthopedic devices are increasingly used to treat fractures and replace joints. While the devices improve mobility and quality of life, infection is a significant risk in spite of improvements in surgical procedures (e.g., short operating times, clean room environment and administration of perioperative local antibiotic prophylaxis). In the US, about 2 million fracture-fixation devices are inserted annually, and nearly 5% of these become infected with an average estimated cost of $15,000 for medical and surgical treatment together.[1,2] Open fractures have higher chances of infection after fixation (>30%) as compared to closed fractures (1-2%);[3,4,5] other risk factors include diabetes, smoking, and immunodeficiency states. Implants increase both the risk and severity of infections as pathogens can form biofilms on implants which are resistant to antibiotics and the host's immune system. If the infection can be diagnosed near its onset, treatment through surgical debridement and antibiotics without implant removal is often successful;[6] however, mature biofilms usually require implant removal followed by re-insertion of the medical device after the infection is eradicated.[7,8] Sensors are needed at nidus of infection on the implant surface for early detection monitoring treatment, and for elucidating the local biochemical milieu to rationally develop therapeutics.

Common signs of infection include fever, pain, redness, swelling, as well as elevated blood levels of C-reactive protein (CRP) and erythrocyte sedimentation rates (ESR), but these are not specific for implant infection and can also occur for systemic infection.[9] Another challenge is to differentiate between septic and aseptic loosening of implant and in the case of chronic infection, clinical signs and symptoms of infection may be entirely absent.[10] Histopathological testing of intraoperative tissue, radiology and bone scans are all used in conjunction to diagnose implant associated infection but lack high sensitivity and specificity.[11] In many cases, infections are diagnosed based on sinus tracts, discharge,

radiolucence near implants, and other signs and symptoms, but there are also cases where physicians are uncertain, even intraoperatively.

We are developing a pH sensor to non-invasively detect, monitor, and study implant associated infection in situ using X-ray excited luminescence chemical imaging (XELCI). pH is selected as target analyte because local acidosis (from the acidic products from bacterial metabolism and immune cells) cause a drop in pH, especially in dormant and poorly perfused regions, and is indicative of infection.[12,13] Local acidosis plays a role in immune response and antibiotic effectiveness, and is a potential therapeutic target based on drug release in infected acidic regions, or pH restoration.[14] It is also a potential indicator for implant infection diagnosis and monitoring. pH in infection has been reported to depend on the environment, for example, in well mixed synovial joint fluid, it correlates with white blood cell count and threshold for infection is decrease from pH 7.5 to 7.[15] In osteomyelitis or implant loosening, it can drop to as low as pH 4 and cause formation of brushite and bone erosion[16, 17, 18] while within the biofilm it maybe heterogeneous with local acidosis at base of biofilm even if surroundings are neutral.[19] Since the behavior depends on the context, sensors are needed at nidus of persistent infection at the surface of the implant under the biofilm to detect, understand and treat the infection.

XELCI uses a combination of focused X-ray excitation and optical emission to image chemical concentrations on the surface of implanted sensors which can be coated or attached to implanted medical devices. When the sensors are irradiated with an X-ray beam, the sensor's scintillator layer generates luminescence and its pH-indicator film absorbs some of this light which modulates the spectrum according to pH. The approach combines the chemical sensitivity and surface specificity of an optical pH indicator film with the low background and high spatial resolution of scanning X-ray excited optical luminescence imaging. A variety of luminescence studies have been performed with optical sensor films based on fluorescence,[20–23] surface enhanced Raman spectroscopy (SERS),[24] upconversion,[25–27] and other techniques that can respond to various physical and chemical stimuli such as pH, temperature, pressure, ions, light and humidity.[28] While these can provide average chemical measurements, optical scattering of the excitation and emission light in thick tissue limits the spatial resolution and is approximately the depth of the tissue or worse.[29] This low resolution prevents observation of small and localized acidic regions during infection and treatment or spatially distinct sensor and reference regions to account for spectral distortion and detect multiple analytes with multiple sensors.

In previous studies, we have shown proof of principle for XELCI measurement of pH concentrations in silica-coated glass slides imaged in vitro through 6 mm of chicken breast tissue using a microscope-coupled spectrograph.[30] We were able to observe a spatially separate sensor region and observed a pH drop during in vitro bacterial culture followed by pH neutralization after antibiotic treatment.[30] Herein we developed a clip that can be added to an orthopedic tibial plate with a more robust hydrogel-based sensor, developed a dedicated scanning X-ray system measuring optical transmittance at two wavelengths, studied effect of chicken breast tissue thickness up to 19 mm thick, and demonstrated imaging on a human cadaveric tibia (which is larger, has more attenuating tissue, and more medically relevant). By more efficiently collecting light and scanning, the system could

acquire 40 x 40 mm^2 images in 15 minutes with a pixel size of 300 μm at a higher spatial resolution and through thicker samples compared to a 7.5 x 7.5 mm^2 image in the same time with a microscope (over 20-fold faster). The hydrogel was far more robust than the fragile glass coverslip previously used. Unlike the microscope system, the sample was imaged from the same side as the incident X-ray, and sample size could be increased to allow imaging of cadaveric samples and future rabbit studies.

EXPERIMENTAL DETAILS

All experiments were performed at room temperature and atmospheric pressure unless noted otherwise. All chemical reagents were purchased from Sigma-Aldrich (St. Louis, MO) and standard buffer solutions from VWR (Radnor, PA) unless otherwise indicated.

Sensor Fabrication.

The sensor consists of two layers. A bottom layer of scintillator particles (Gd2O2S:Eu) encapsulated in polydimethylsiloxane (PDMS), and a pH-sensitive top layer synthesized from biocompatible polyethylene glycol (PEG) hydrogel incorporating the pH-indicator dye bromocresol green (BCG). Both the pH-sensing film and scintillating particles are placed in a 3D printed holder made from polylactic acid (PLA) that can be attached to the orthopedic plate.

Scintillator layer: Silicone elastomer and curing agent (SYLGARD™ 184 Silicone Elastomer base and curing agent, Dow Corning, Midland, Michigan, United States) were mixed in 10:1 (w/w) ratio and ~8.0 μm diameter Gd2O2S:Eu scintillator particles (UKL63/N-R1, Phosphor Technologies Inc., Stevenage, England) were added in 5:1 (w/w) ratio to form a final mixture of 5 g scintillator particles per 1 g of PDMS. This mixture was spread on a glass slide and cured in the oven at 100 °C to form about 1 mm thick scintillator-PDMS layer. It was cut into either 5 mm or 7 mm discs using a hole puncher.

pH sensitive layer: To synthesize the hydrogel films, a solution was prepared containing 79% (w/w of sol.) 700 MW polyethylene glycol diacrylate (PEGDA), 9.9% (w/w of sol.) glycerol, 9.9% (w/w of sol.) water, 0.8% (w/w of sol.) photoinitiator (2,2-dimethoxy-2-phenylacetophenone) and 0.4% (w/w of sol.) bromocresol green (pH-indicating dye). This mixture was stirred on a magnetic plate for 30 minutes and the resulting solution was drop coated and sandwiched between two clean cover slips and cured under UV for 2 minutes. The films were immersed in water to swell and delaminate from the coverslips and washed several times before cutting into discs of desired size using hole punchers.

Characterization of pH-indicating film: Spectra were obtained for the pH dye free in solution and encapsulated in the hydrogel at different pH. For the free dye, a solution of the dye was prepared in ethanol (1 mg/ml) and 20 μl of this dye solution was added to 2 ml of standard buffers of pH 3-8 and spectra obtained. A 96 well plate was prepared with the pH film samples kept in 100 μl of each pH buffer solution from pH 3 to 8 for at least two hours to reach maximum response and spectra obtained for each pH with a spectrometer (DNS 300, DeltaNu, Laramie, WY, United States). For reversibility study, a 5 mm pH film was fixed to a sample holder and cycled between pH 4 and phosphate saline

(~pH 7.2) buffers. Spectra was acquired on the same spectrometer every 1 second for a total of 30 minutes in each buffer and repeated for 5 cycles. To measure the attenuation of the scintillator emission signal by the pH dye, the sensor (a piece of pH film covered by scintillator film) immersed in standard buffer solution was placed on the stage of an inverted microscope (DMI 5000, Leica Microsystems, Germany) and irradiated with a focused X-ray beam. The pH modulated emission of the scintillator film was collected by a 5× objective lens and focused to a spectrometer (DNS 300, DeltaNu, Laramie, WY, USA), equipped with a cooled CCD camera (iDUS-420BV, Andor, South Windsor, CT, United States). Spectra were collected for each pH after immersing the pH film in the respective buffers.

XELCI Setup.

Figure 1 shows the setup schematic. The sample is placed on an x-y-z motorized stage with 30 x 15 x 6 cm travel (Models: LTS300 and LTS150, Thorlabs Inc., Newton, NJ, USA for x and y axis and Motorized Linear Vertical Stage Model AT10-60, Motion Control, Smithtown, NY, USA for the z-stage) and positioned under the focused X-ray beam (iMOXS, Institute for Scientific Instruments GmbH, Berlin, Germany) and detecting optics.

An X-ray beam is focused using a polycapillary lens (5 cm focal distance from capillary tip) and excites the scintillator particles generating luminescence. This luminescence passes through the pH-indicating film which modulates the spectrum according to pH, and some of the light diffuses through the tissue where it is collected using a liquid light guide (Model 77638, Newport Corporation, Irvine, CA, United States), collimated with a lens, and directed to a beam splitter. The beam splitter sends the light to two photomultiplier tubes (PMTs) (Model P25PC-16, SensTech, Surrey, UK) with a band pass filter in front of each (one passing 620 nm light, the other passing 700 nm). The whole setup is enclosed in a light-tight box. Pulses from each PMT are counted using a Data Acquisition (DAQ) board (NI cDAQ™-9171, National Instruments, Austin, TX). The stage position is controlled with a program written in LabVIEW (National Instruments, Austin, TX), which also records PMT counts and stage position versus time, and displayed an image on the computer screen during acquisition. The scanning process and signal processing is explained in our previous work.[31]

Imaging through Tissue.

Chicken breast tissue was cut into slices of desired thickness using an electric food slicer (Model 630, Chef's Choice, Avondale, PA, USA). A 5 mm thick slice of chicken breast tissue was wrapped in clear plastic and placed on the stage. The 3D printed holder containing 5 pH sensor discs (in pH buffers 4, 5, 6, 7 and 8) and a reference disc as well as a reference strip was placed on top of the tissue and scanned from the top using XELCI. The XELCI imaging was repeated after adding another slice of chicken breast tissue (either 1, 3, 5, 7, 9, 11, 13, 15, 17 or 19 mm thick) over top of the sensor. From this data, calibration curves could be plotted showing peak ratio and intensity vs. pH and depth.

Imaging through Human Cadaveric Tissue.

The pH sensor discs were placed in a 3D printed holder and incubated with pH 4, 5, 6, 7, and 8 using respective pH buffers. The holder was attached on a tibial orthopedic plate affixed to a cadaveric human tibia with an induced fracture. The cadaveric tissue covering the top of the orthopedic plate was cut off to allow for imaging of the sensor discs without tissue. This tissue flap (about 11 mm thick) was then placed back over the sensor discs and imaged again using XELCI to obtain the signal intensity at each pH through the human cadaveric tissue.

pH Reversibility.

To observe reversible pH changes through the tissue, two adjacent wells on the 3D printed holder were selected. One well contained the reference disc (with no pH film) and the second well contained a pH sensor disc. The pH of the second well containing the pH sensor disc was cycled between pH 4 and pH 7 using the respective pH buffers to show reversibility imaged through the human cadaveric tissue using XELCI for each case.

Data Analysis.

A custom Labview program controls the motorized stage and collects both stage position versus time and photon counts versus time for the 620 nm and 700 nm PMTs. From this raw data, custom Matlab scripts allocate the photon counts per second to specific pixels based on the motor position at the time acquired. The 620 nm and 700 nm signal intensities were displayed as pseudo-colored images after background subtraction for each data set. Ratiometric images were displayed in a similar manner; a threshold intensity at 620 nm and 700 nm used to avoid showing highly noisy pixels. To plot the calibration curves, the average signal intensity for each pH-sensor disc in its particular pH buffer, the 620 nm, 700 nm intensity and ratio was calculated for each chicken slice thickness (0 – 19 mm) and through the human cadaveric tissue. The ratios were then normalized to the reference disc signal for each data set and plotted as a calibration curve on a single graph. Normalization is done by dividing the average ratio values for each pH disc by the average ratio value of the reference disc for the respective tissue thicknesses.

RESULTS AND DISCUSSION

Sensor Characterization.

The sensor attaches to an implant surface and has two components: an X-ray scintillator layer (Gd_2O_2S:Eu microphosphors in a PDMS film) covering a metal implant surface (or clip which can attach to an implant), and a pH-sensitive film (bromocresol green in a PEG hydrogel) covering the scintillator film (Figure 2a). Under irradiation, the X-ray excited optical luminescent signal has very low background from tissue unlike most fluorescence-based measurements through tissue.[32] The luminescence spectrum is modulated by the pH indicator film: In neutral and basic conditions, the bromocresol green film appears blue and strongly absorb 620 nm light from the scintillators, while in acidic media, the film appears yellow and transmits most 620 nm light (Figure 2b); absorption at 700 nm is minimal regardless of pH. Figure 2c shows how this pH-dependent absorption modulates

the X-ray excited luminescence spectrum acquired through the indicator layer. Taking a ratio between 620 nm and 700 nm peaks normalizes the data to account for pH-independent variation in X-ray intensity and optical collection efficiency. Figure 2c inset shows peak ratio versus pH. The sensor has a range from pH 4-8 which is physiologically relevant. The curve is shifted by about 1 pH unit compared to free dye because the hydrogel alters the local microenvironment and effective pK_a[24,33] Interestingly, after encapsulation we observe a small spectral blue-shift to the protonated absorption peak and a red-shift to the deprotonated peak. This indicates that the dye in the gel experience a different local environment which affects the absorption photophysics, although we do not know the specific mechanism. Full absorption spectra of the film and dye as a function of pH and the inset of ratio vs. pH (log scale) are shown in electronic supporting information Figures S1 and S2. The sensor is reversible and has a $\tau_{90\%}$ time constant of approximate 25 minutes going from pH5 to pH 7.4 and 5 minutes going from pH 7.4 to pH 5 (Figure S4 in ESI), which is adequate for most in vivo applications where pH shifts over hours.

We designed the sensor using biocompatible materials minimizing the toxicity associated with potential leaching of the pH indicator dye, and photoinitiator by an initial pre-leaching treatment. PEG is widely used in tissue engineering applications because of its hydrophilicity, resistance to protein adsorption and customizability by modification of the chain length and addition of functional groups.[34,35] The gadolinium particles enclosed in PDMS do not leach out or dissolve even in 1 M sulfuric acid.[30] Gadolinium (Gd) compounds are used as contrast agents in MRI and the amount of Gd used in the sensor (18 mg of Gd2O2S:Eu per 1 cm^2 of area) is less than the recommended dose for MRI (0.1 mM of Gd-chelate per kg of body weight).[36] The sensor leaches less than 10% of dye in PBS in 36 days (ESI, Figure S3).

Effect of Tissue Thickness on Signal Intensity.

pH calibration curves were collected through a series of chicken breast tissue thicknesses (0-19 mm). Six 5 mm sensor discs were placed together on a clip and imaged using XELCI: one disc was a spectral reference with no pH-indicator film; the other five discs were pH-sensors in standard pH buffers at pH 4.0, 5.0, 6.0, 7.0, and 8.0 (Figure 3). The discs changed color from yellow at low pH to blue at high pH, with a white reference disc with no pH film (Figure 3a). Similarly, the XELCI 620/700 nm ratio images show decreasing ratio going from acid to base (increasingly blue in pseudo-colored ratio images, Figure 3c). When the clip was covered with tissue, the tissue obscured the clip from view in the photo, but the clips were readily apparent in the XELCI ratio image. With increasing tissue thickness, the 620 nm/700 nm ratio decreased at all pH (due to stronger tissue absorption at 620 nm), evident as a "blue shift" in the pseudo colored ratio images. The underlying 620 nm and 700 nm images are shown in ESI Figure S5, and the average values are shown in Figure 4. Absolute intensity depends on several factors including alignment of optics, PMT sensitivity, scintillator film thickness and tissue thickness/properties. However, the spectral peak ratio accounts for these variations. For example, Figure 4a&b shows that both 620 and 700 nm light was above the trendline intensity through 9 mm of tissue, (about 1.4 times higher than expected at pH 4); however, the ratio of 620 nm to 700 nm light was consistent with other curves (Figure 4c&d). At any given thickness, the sensors in basic media consistently

absorbed more 620 nm than 700 nm light and the 5 mm diameter discs were clear through even 19 mm of tissue.

To quantify how the 620 nm, 700 nm and ratio signal changed with tissue thickness, we calculated the average intensity for each pH disc (Figure 4). Luminescence intensity at both wavelengths decreased exponentially with tissue thickness due to a combination of X-ray attenuation and optical absorption in the tissue (with a long path length due to multiple optical scattering events). The 620 nm light was more rapidly attenuated: After passing through 19 mm of tissue, the reference disc's average luminescence intensity decreased to 2.6% of its intensity without tissue at 620 nm, and to 6.1% at 700 nm. Similar attenuation was observed for all the pH-indicating discs (Figure 4c). This spectral distortion implies that tissue has a higher effective attenuation coefficient, μ_{eff}, at 620 nm than 700 nm, which is expected from its higher underlying absorption coefficient, μ_a, and slightly higher reduced scattering coefficient, μ_s. For example, Marquez and co-workers found that μ_{eff} in chicken breast tissue depended on the sample and muscle fiber orientation but ranged between 0.56 – 1.28 cm^{-1} at 620 nm with an average of 0.99 cm^{-1} and 0.35 – 0.85 cm^{-1} at 700 nm with an average of 0.57 cm^{-1}.[37] These average values suggest a loss of 1.74 times more at 620 vs 700 nm per cm and is consistent with the chicken data reference intensity values observed in our experiments corresponding to a loss of 1.58 – 1.95 times in going from 0 to 9 mm and from 0 to 11 mm of chicken tissue, respectively.

Since the spectral distortion at any given tissue thickness was consistent for all pH, the reference disc spectrum could be used to measure and account for this distortion. The reference disc consists of only scintillator layer without a pH sensitive gel layer and is not affected by pH changes, it can be used to account for signal attenuation caused by the tissue. This pH independent attenuation is same for sensor discs and reference disc as long the tissue is uniform. The ratio at each tissue thickness was normalized to the ratio measured for the reference disc ratio (Figure 4d). These normalized calibration curves overlap well with each other allowing a tissue depth-independent calibration. This normalization is effective provided the tissue is homogeneous over the distance between the sample and the reference. The standard deviation in normalized ratio at different tissue thicknesses corresponded to about 0.2 pH units between pH 4-8.

The pixel-to-pixel noise level within any disc could be found by dividing the ratio standard deviation the by calibration curve slope. This noise depended strongly on the light intensity at 620 nm and increased with both pH and tissue depth: At 1 mm tissue the noise ranged from 0.015 pH units at pH 4 to 0.17 at pH 7; at 11 mm, it ranged from 0.067 at pH 4 to 0.54 at pH 7; and at 19 mm it ranged from 0.12 pH units at pH 4 to 1.4 pH units at pH 7. The signal to noise ratio (S/N) appeared to be limited by shot noise at low 620 nm signal intensity (10–100 counts per pixel at 620 nm) implying increasing signal intensity/pixel would increase the S/N (Supporting Information Figure S6). This could be achieved by slowing acquisition, averaging over several of the 250 μm pixels, optimizing the pH film for a given pH (e.g., less dye would give better resolution at higher pH), or improving the optical collection and detection efficiency of the setup. Nevertheless, the results showed reasonably good pH resolution even through 19 mm of tissue at low pH or averaged across a disc.

Cadaver Study.

The pH sensors were next imaged with XELCI on a human cadaveric lower leg. A series of pH sensor discs were prepared in a similar manner except that the pH indicating film was pre-leached in the buffer for several days resulting in slightly shifted pH spectra as the excess dye leached out. Figure 5a shows a photograph of the pH discs that were placed on an orthopedic plate fixed on the cadaveric human tibia and imaged through the tissue and skin. The reconstructed XELCI images for both 620 nm and 700 nm intensities as well their ratio (I6/I7) through the cadaveric tissue are shown in Figure 5b and the calibration curve is shown in Supporting Information Figure S7. The image has high spatial resolution (like Figure 3 through chicken breast) due to the sharp focus of the incident X-ray beam. Analysis of the XELCI images reveal a spatial resolution (80%-20% knife edge resolution) of about 500 μm for both the 620 and 700 nm signal intensities through tissue. XELCI has sub-millimeter spatial resolution that is comparable to most of the radiation based imaging techniques such as X-ray projection computed tomography (typical spatial resolution of about 0.5 mm for medical CT systems and higher for μCT), single photon emission computed tomography (spatial resolution of 15–20 mm for a SPECT of human brain) and positron emission tomography (spatial resolution of 1–3 mm for μ-PET and 5–10 mm for clinical PET). Usually, there is a tradeoff between high spatial resolution, sensitivity, energy of the X-rays used and radiation dose.[38] This X-ray beam-limited spatial resolution is much finer than the optical point spread function (which is typically over 10 mm for imaging through 10 mm of tissue),[29] allowing the sample signal to be distinguished from reference region signal and enabling visualization of fine pH features in the sample.

Reference and acidic pH discs appear brighter and the higher pH discs are less intense except for pH 8 that was on the edge with light leaking out as the tissue could have been thinner or a good possibility that it was not properly covered all the way on that end. The pH discs closer to the reference are also normalized better than those away from the reference and again this effect is especially pronounced for pH 8. This is because the cadaveric tissue was not uniform over the whole length of the sensor discs as can be seen in the 700 nm intensity image and changes in tissue thickness affects signal normalization. The 700 nm intensity can be used to address tissue discrepancies.

Although the calibration curve in the cadaveric specimen was similar to the chicken breast tissue, the signal intensity ratio was 5 times weaker for the same tissue depth (a distortion factor of 5x for chicken tissue as compared to 25x for cadaveric tissue) and the overall signal intensity was much lower too. This is qualitatively consistent with reported absorption values in literature for human muscle tissue (for example, μ_a value of 11.2 cm^{-1} at 633 nm) compared to the white chicken tissue (μ_a value of 0.12 – 0.17 cm^{-1} at 633 nm) mainly because of absorption by blood and also depends on the measurement and modelling techniques used.[39] Covering the sensors with 11 mm of cadaveric tissue decreases the signal by 1600x at 620 nm and 140x at 700 nm, more than expected based solely on in vivo extinction coefficient of human extremities: Taroni et al reported that the 1/e penetration depth of light through a live human forearm (probably similar to lower leg) was 0.26 cm at 620 nm and 0.42 cm at 700 nm, corresponding to an expected plane wave attenuation through 11 mm of tissue of 69x at 620 nm and 15x at 700 nm.[40] The comparatively

weaker signal we observed is likely a combination of incident X-ray attenuation, lateral diffusion of the light to a spot size larger than the 7.6 mm core liquid light guide, and differences in the skin and tissue after freeze thaw cycles. Even with a large attenuation, however, high spatial resolution pH maps were acquired through the tissue in a plated lower leg specimen. Also, the principle of luminescence imaging and referencing through tissue worked for both cadaveric and chicken breast tissue and would apply to any homogeneous tissue sample whether it absorbs and scatters more or less than in a cadaveric specimen. The tray is large enough to accommodate animals as large as rabbits. For such studies, additional considerations would need to be given for shaving the fur, anesthetizing the animal to keep it still during the scan, and using multiple reference regions to account for possible variation in tissue thickness and optical properties; these will be discussed in forthcoming publications.

A plain radiograph of the cadaveric lower leg with the pH sensors affixed to the tibial orthopedic plate was also obtained and super-imposed with a ratiometric XELCI image of the same (figure 5c). This combination of structural (radiograph) and functional (XELCI) X-ray imaging can provide useful information about bone healing and implant associated infection.

To show the changes in pH on the same pH sensor can be imaged through tissue using XELCI, a sensor disc was cycled through pH 4 and pH 7 and scanned through the human cadaveric tissue. pH 4 and 7 were chosen as these represent the two extremes of the pH spectrum with one being neutral/physiological and the other acidic.[30] We also observed a pH drop from pH 7.4 to 5 during the in vitro biofilm study reported in our previous work. Figure 6 shows the XELCI ratiometric images of a reference disc (right) and the cycled pH sensor disc (left). The change in signal intensity indicating the change in pH and reversible response can be clearly seen (consistent with the in vitro reversibility study on the pH sensor film, Figure S4). The intensity ratio for each pH agree with the respective values of the pH calibration curve obtained through the human cadaveric tissue. Placement of flap of the human cadaveric tissue varied each time as the pH discs were cycled between the two pH. This resulted in minor differences in the signal intensities for pH 7 in figure 6a and 6c, and for pH 4 in figure 6b and 6d because of differences in thickness of the cadaveric tissue, the same is also true for the reference disc. This can be accounted for by calculating the difference in intensity values for the reference disc between each measurement.

CONCLUSIONS

We imaged and resolved different pH through human cadaveric tissue and evaluated the effect of increasing tissue (chicken) thickness on the signal from our sensors. Although the tissue attenuates the signal intensity, we were able to resolve different pH through as much as 19 mm thick tissue. The data obtained through the human cadaveric tissue agree with the chicken tissue measurements demonstrating the consistency of sensor response and the imaging technique (XELCI). Sensor design can be modified to develop a method to uniformly coat the whole implant with the pH sensor layers. In addition, the imaging system is far from optimized and optical collection can improved using red-efficient photodetectors (the PMTs were 5% efficient at 620 nm and 2% at 700 nm), and replacing the 7.6 mm core liquid light guide with a larger air/acrylic light guide to increase collection area and

acceptance angle. Further studies will be conducted to measure pH changes on the surface of implanted medical devices in a rabbit model to help diagnose and gain insight into implant associated infection.

Supplementary Material

Refer to Web version on PubMed Central for supplementary material.

ACKNOWLEDGMENT

ABBREVIATIONS

BCG	bromocresol green dye
DAQ	data acquisition
PDMS	poly-dimethylsiloxane
PEG	Polyethylene glycol
PMT	Photomultiplier tube
XELCI	X-ray excited luminescence chemical imaging

REFERENCES

(1). Darouiche RO Treatment of Infections Associated with Surgical Implants. New England Journal of Medicine 2004, 350 (14), 1422–1429. 10.1056/NEJMra035415. [PubMed: 15070792]

(2). Isiklar ZU; Darouiche RO; Landon GC; Beck T Efficacy of Antibiotics Alone for Orthopaedic Device Related Infections. Clin. Orthop. Relat. Res 1996, No. 332, 184–189. [PubMed: 8913162]

(3). McGraw JM; Lim EV Treatment of Open Tibial-Shaft Fractures. External Fixation and Secondary Intramedullary Nailing. J Bone Joint Surg Am 1988, 70 (6), 900–911. [PubMed: 3392088]

(4). Mody RM; Zapor M; Hartzell JD; Robben PM; Waterman P; Wood-Morris R; Trotta R; Andersen RC; Wortmann G Infectious Complications of Damage Control Orthopedics in War Trauma. J Trauma 2009, 67 (4), 758–761. 10.1097/TA.0b013e3181af6aa6. [PubMed: 19820582]

(5). Raahave D Postoperative Wound Infection After Implant and Removal of Osteosynthetic Material. Acta Orthopaedica Scandinavica 1976, 47 (1), 28–35. 10.3109/17453677608998968. [PubMed: 1266589]

(6). Trampuz A; Widmer AF Infections Associated with Orthopedic Implants. Curr. Opin. Infect. Dis. 2006, 19 (4), 349–356. 10.1097/01.qco.0000235161.85925.e8. [PubMed: 16804382]

(7). Widmer AF New Developments in Diagnosis and Treatment of Infection in Orthopedic Implants. Clin. Infect. Dis 2001, 33 Suppl 2, S94T06. https://doi.oig/10.1080/321803. [PubMed: 11486305]

(8). Broekhuizen C. a. N.; Sta M; Vandenbroucke-Grauls CMJE; Zaat S. a. J. Microscopic Detection of Viable Staphylococcus Epidermidis in Peri-Implant Tissue in Experimental Biomaterial-

Associated Infection, Identified by Bromodeoxyuridine Incorporation. Infect. Immun. 2010, 78(3), 954–962. https://doi.oig/10.1128/IAI.00849-09. [PubMed: 20048041]

(9). Piper KE; Femandez-Sampedro M; Steckelbeig KE; Mandrekar]N; Karau M]; Steckelbeig]M; Berbari EF; Osmon DR; Hanssen AD; Lewallen DG; et al. C-Reactive Protein, Erythrocyte Sedimentation Rate and Orthopedic Implant Infection. PLoS ONE 2010, 5 (2), e9358. https://doi.oig/10.1371/journal.pone.0009358. [PubMed: 20179760]

(10). Konttinen YT; Takagi M; Mandelin]; Lassus]; Salo]; Ainola M; Li T-F; Virtanen I; Liljestrom M; Sakai H; et al. Acid Attack and Cathepsin K in Bone Resorption Around Total Hip Replacement Prosthesis. Journal of Bone and Mineral Research 2001, 16 (10), 1780–1786. https://doi.oig/10.1359/jbmr.2001.10.10.1780. [PubMed: 11585341]

(11). Trampuz A; Zimmerli W Diagnosis and Treatment of Infections Associated with Fracture-Fixation Devices. Injury 2006, 37 Suppl 2, S59–66. https://doi.oig/10.1016/j.injury.2006.04.010.

(12). Stewart PS; Costerton JW Antibiotic Resistance of Bacteria in Biofilms. The Lancet 2001, 358 (9276), 135–138. 10.1016/S0140-6730(01)05321-1.

(13). Grinstein S; Swallow CJ; Rotstein OD Regulation of Cytoplasmic PH in Phagocytic Cell Function and Dysfunction. Clin. Biochem 1991, 24 (3), 241–247. [PubMed: 1651820]

(14). Erra Diaz F; Dantas E; Geffner] Unravelling the Interplay between Extracellular Acidosis and Immune Cells. Mediators Inflamm 2018, 2018. 10.1155/2018/1218297.

(15). Ward TT; Steigbigel RT Acidosis of Synovial Fluid Correlates with Synovial Fluid Leukocytosis. The American Journal of Medicine 1978, 64 (6), 933–936. https://doi.oig/10.1010/0002-9343(78)90440-1. [PubMed: 26220]

(16). Esmonde-White KA; Esmonde-White FWL; Holmes CM; Morris MD; Roessler BJ Alterations to Bone Mineral Composition as an Early Indication of Osteomyelitis in the Diabetic Foot. Diabetes Care 2013, 36 (11), 3652–3654. 10.2337/dc13-0510. [PubMed: 23920085]

(17). Abu-Amer Y; Darwech I; Clohisy JC Aseptic Loosening of Total Joint Replacements: Mechanisms Underlying Osteolysis and Potential Therapies. Arthritis Res Ther 2007, 9 (Suppl 1), S6. https://doi.oig/10.1186/ar2170.

(18). Konttinen YT; Takagi M; Mandelin J; Lassus J; Salo J; Ainola M; Li T-F; Virtanen I; Liljestrom M; Sakai H; et al. Acid Attack and Cathepsin K in Bone Resorption Around Total Hip Replacement Prosthesis. Journal of Bone and Mineral Research 2001, 16 (10), 1780–1786. 10.1359/jbmr.2001.16.10.1780. [PubMed: 11585341]

(19). Hidalgo G; Bums A; Herz E; Hay AG; Houston PL; Wiesner U; Lion LW Functional Tomographic Fluorescence Imaging of PH Microenvironments in Microbial Biofilms by Use of Silica Nanoparticle Sensors. Appl. Environ. Microbiol 2009, 75 (23), 7426–7435. https://doi.oig/10.1128/AEM.01220-09. [PubMed: 19801466]

(20). Dansby-Sparks RN; Jin J; Mechery SJ; Sampathkumaran U; Owen TW; Yu BD; Goswami K; Hong K; Grant J; Xue Z-L Fluorescent-Dye-Doped Sol–Gel Sensor for Highly Sensitive Carbon Dioxide Gas Detection below Atmospheric Concentrations. Anal. Chem 2010, 82 (2), 593–600. https://doi.oig/10.1021/ac901890r. [PubMed: 20038093]

(21). Li Z; Liang R; Liu W; Yan D; Wei M A Dual-Stimuli-Responsive Fluorescent Switch Ultrathin Film. Nanoscale 2015, 7 (40), 16737–16743. https://doi.oig/10.1039/C5NR05370E. [PubMed: 26400734]

(22). Yang Y; Wang K-Z; Yan D Ultralong Persistent Room Temperature Phosphorescence of Metal Coordination Polymers Exhibiting Reversible PH-Responsive Emission. ACS Appl. Mater. Interfaces 2016, 8 (24), 15489–15496. https://doi.oig/10.1021/acsami.0b03950. [PubMed: 27253185]

(23). Zhang Y; Li S; Pan G; Yang H; Qile M; Chen J; Song Q; Yan D Stretchable Nanofibrous Membranes for Colorimetric/Fluorometric HC1 Sensing: Highly Sensitive Charge-Transfer Excited State. Sensors and Actuators B: Chemical 2018, 254, 785–794. https://doi.oig/10.1016/j.snb.2017.07.040.

(24). Surface-Enhanced Raman Scattering Detection of pH with Silica-Encapsulated 4-Mercaptobenzoic Acid-Functionalized Silver Nanoparticles-Analytical Chemistry (ACS Publications) https://pubs.acs.org/doi/full/10.1021/ac3018179?src=recsys (accessed May 7, 2019).

(25). Chen H; Qi B; Moore T; Wang F; Colvin DC; Sanjeewa LD; Gore JC; Hwu S-J; Mefford OT; Alexis F; et al. Multifunctional Yolk-in-Shell Nanoparticles for PH-Triggered Drug Release and Imaging. Small 2014, 10 (16), 3364–3370. https://doi.oig/10.1002/smll.201303709. [PubMed: 24753264]

(26). Wang F; Raval Y; Chen H; Tzeng T-RJ; DesJardins JD; Anker JN Development of Luminescent PH Sensor Films for Monitoring Bacterial Growth Through Tissue. Advanced Healthcare Materials 2014, 3 (2), 197–204. 10.1002/adhm.201300101. [PubMed: 23832869]

(27). Mahata MK; Bae H; Lee KT Upconversion Luminescence Sensitized PH-Nanoprobes. Molecules 2017, 22 (12), 2064. https://doi.oig/10.3390/molecules22122064. [PubMed: 29186844]

(28). Gao R; Fang X; Yan D Recent Developments in Stimuli-Responsive Luminescent Films. Journal of Materials Chemistry C 2019, 7 (12), 3399–3412. https://doi.oig/10.1039/C9TC00348G.

(29). Shimizu K; Tochio K; Kato Y Improvement of Transcutaneous Fluorescent Images with a Depth-Dependent Point-Spread Function. Appl. Opt., AO 2005, 44 (11), 2154–2161. https://doi.oig/10.1304/AO.44.002154.

(30). Wang F; Raval Y; Tzeng T-RJ; Anker JN X-Ray Excited Luminescence Chemical Imaging of Bacterial Growth on Surfaces Implanted in Tissue. Advanced Healthcare Materials 2015, 4 (6), 903–910. https://doi.oig/10.1002/adhm.201400085. [PubMed: 25611007]

(31). Benza D; Uzair U; Raval Y; Tzeng T-RJ; Behrend CJ; Anker JN X-Ray Excited Luminescent Chemical Imaging (XELCI) for Non-Invasive Imaging of Implant Infections. In Frontiers in Biological Detection: From Nanosensors to Systems IX; International Society for Optics and Photonics, 2017; Vol. 10081, p 100810K. https://doi.oig/10.1117/12.2250049.

(32). Troy T; Jekic-McMullen D; Sambucetti L; Rice B Quantitative Comparison of the Sensitivity of Detection of Fluorescent and Bioluminescent Reporters in Animal Models. 2004, 3 (1), 15.

(33). Yamaguchi A; Namekawa M; Kamijo T; Itoh T; Teramae N Acid–Base Equilibria inside Amine-Functionalized Mesoporous Silica. Analytical Chemistry 2011, 83 (8), 2939–2946. 10.1021/acl02935q. [PubMed: 21417214]

(34). Qiu Y; Park K Environment-Sensitive Hydrogels for Drug Delivery. Advanced Drug Delivery Reviews 2012, 64, 49–60. 10.1016/j.addr.2012.09.024.

(35). Wu Y; Joseph S; Aluru NR Effect of Cross-Linking on the Diffusion of Water, Ions, and Small Molecules in Hydrogels. J. Phys. Chem. B 2009, 113 (11), 3512–3520. 10.1021/jp808145x. [PubMed: 19239244]

(36). Penfield JG; Reilly RF What Nephrologists Need to Know about Gadolinium. Nat Clin Pract Nephrol 2007, 3 (12), 654–668. 10.1038/ncpneph0660. [PubMed: 18033225]

(37). Marquez G; Wang LV; Lin S-P; Schwartz JA; Thomsen SL Anisotropy in the Absorption and Scattering Spectra of Chicken Breast Tissue. Appl. Opt., AO 1998, 37 (4), 798–804. 10.1364/AO.37.000798.

(38). Chen H; Rogalski MM; Anker JN Advances in Functional X-Ray Imaging Techniques and Contrast Agents. Phys. Chem. Chem. Phys 2012, 14 (39), 13469–13486. 10.1039/C2CP41858D. [PubMed: 22962667]

(39). Cheong WF; Prahl SA; Welch AJ A Review of the Optical Properties of Biological Tissues. IEEE Journal of Quantum Electronics 1990, 26 (12), 2166–2185. https://doi.org/10.1109/3.64354.

(40). Taroni P; Pifferi A; Torricelli A; Comelli D; Cubeddu R In Vivo Absorption and Scattering Spectroscopy of Biological Tissues. Photochem. Photobiol. Sci 2003, 2 (2), 124–129. 10.1039/B209651J.
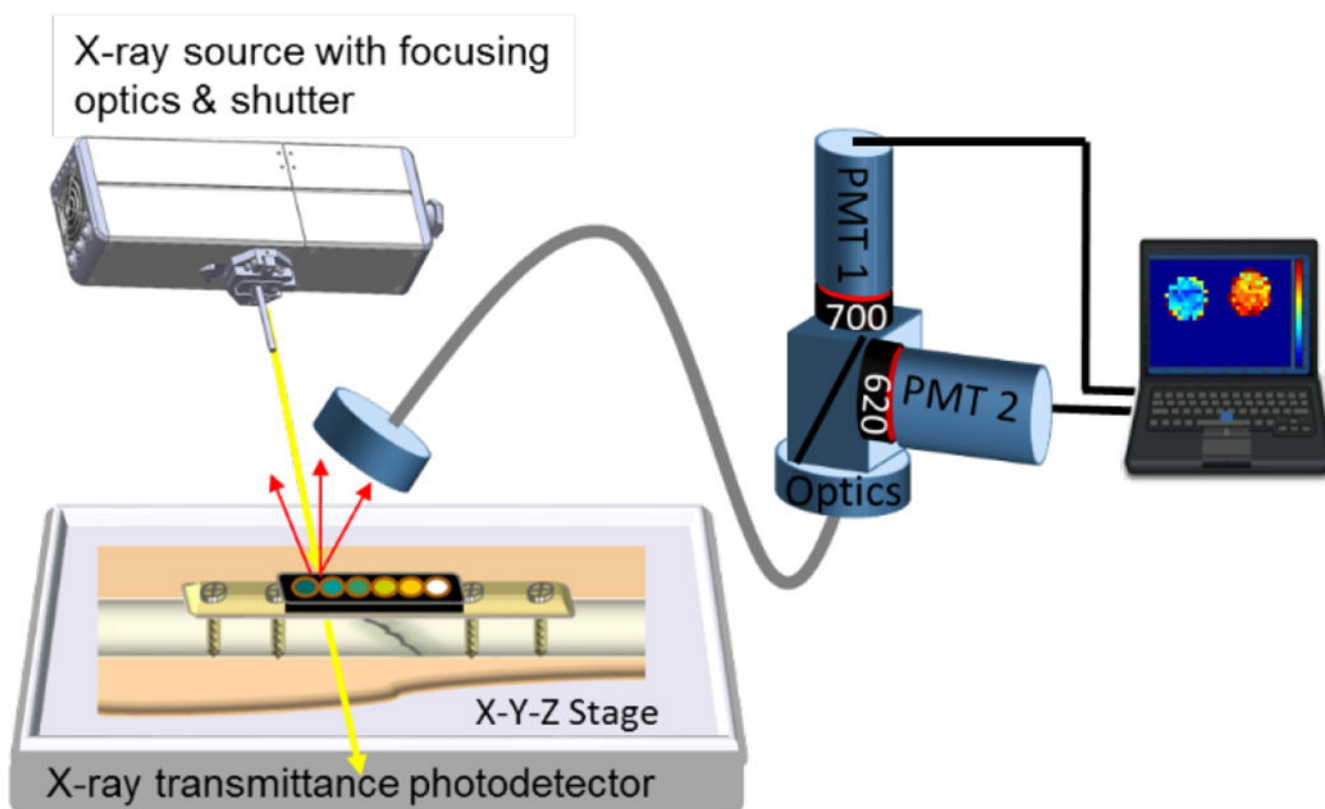
Figure 1.
Schematic drawing of the XELCI experimental setup. The sample is placed on an x-y-z
motorized stage and irradiated with a focused X-ray beam. The luminescence signal is
transmitted via liquid light guide to two photomultiplier tubes (PMTs), measuring light
intensity at 620 nm and 700 nm respectively. The intensities and ratios are monitored as the
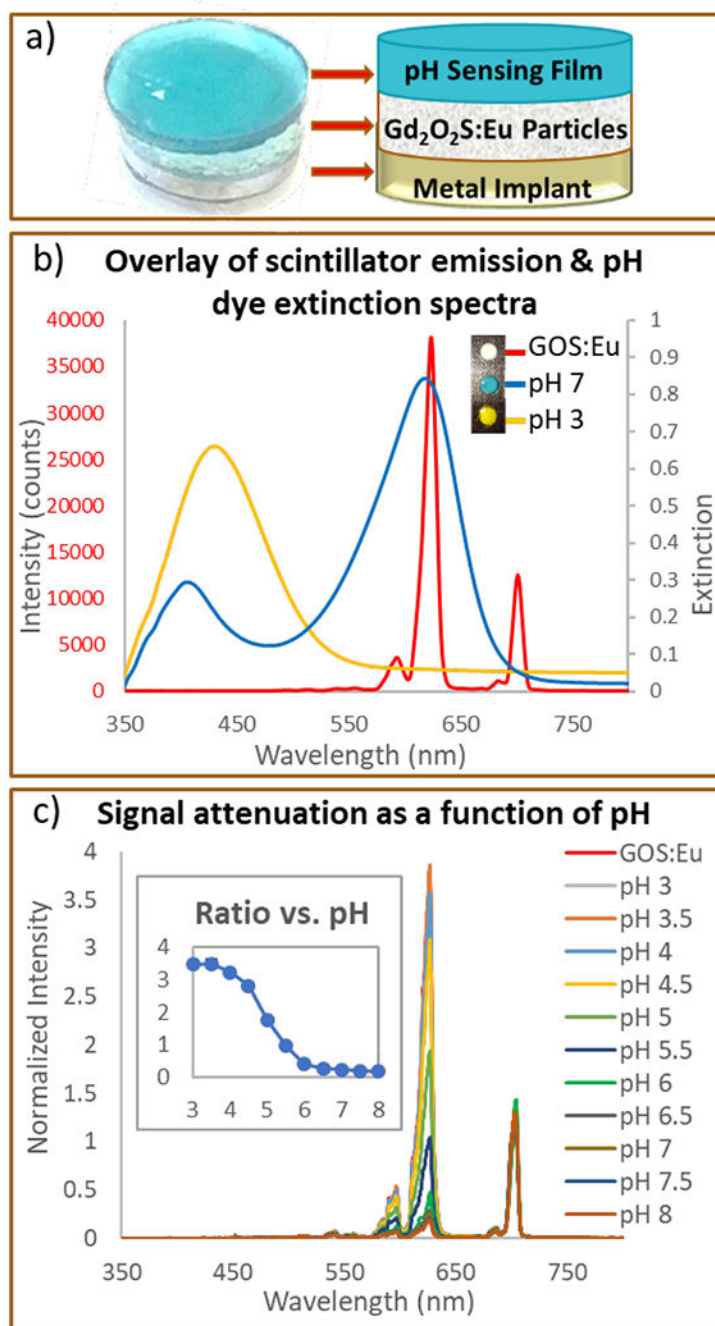stage scans, with real time image shown on the computer screen.

Figure 2.
Sensor design. (a) The sensor consists of two layers: A top pH-indicating film made
of PEG hydrogel with encapsulated BCG dye. A bottom layer of scintillating particles
(Gd_2O_2S:Eu) encapsulated in PDMS and covered by the pH sensing film. (b) Luminescence
spectrum of scintillators (Gd_2O_2S:Eu) (red line, left y-axis) and the extinction spectra of
BCG-doped PEG films in pH 3.0 buffer (yellow line, right y-axis) and pH 7.0 buffer (blue
line, right y-axis). Inset: Sensor discs (scintillator + pH film) showing color change at
acidic pH (yellow), physiological pH (blue-green) and reference disc (white) containing only

scintillators with no pH film covering it. (c) Scintillator radioluminescence spectrum after passing through the BCG pH dye in PEG hydrogel at different pH. Inset: Ratio of 620 and 700 nm intensities plotted for each pH (ratio vs. pH on log scale available in ESI, S2).
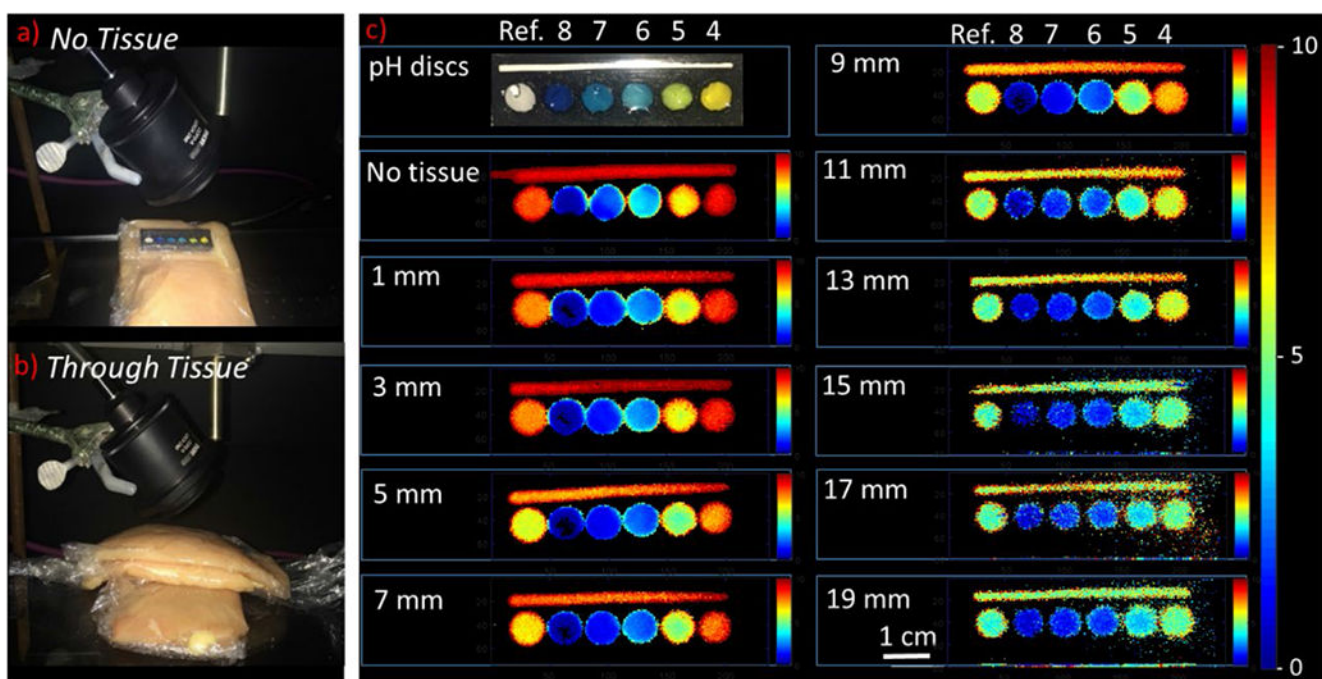
Figure 3.
Imaging pH through varying tissue thickness. (a) Photo of pH sensor discs placed on a piece of tissue. (b) Photo of pH sensor discs sandwiched between two slices of chicken breast tissue. Thickness of the top slice was increased from 1 – 19 mm with 2 mm intervals. (c) Photograph of pH sensor discs (7 mm in diameter) placed in a 3-D printed holder in pH buffers 8, 7, 6, 5 and 4 and a reference disc without any pH coating. A reference strip is placed along the length of the holder to account for variation in signal intensity caused by variation in tissue thickness. Ratiometric XELCI images (ratio of 620 nm and 700 nm intensities) of the pH sensor discs at respective pH obtained without tissue and through 1 – 19 mm of chicken tissue.
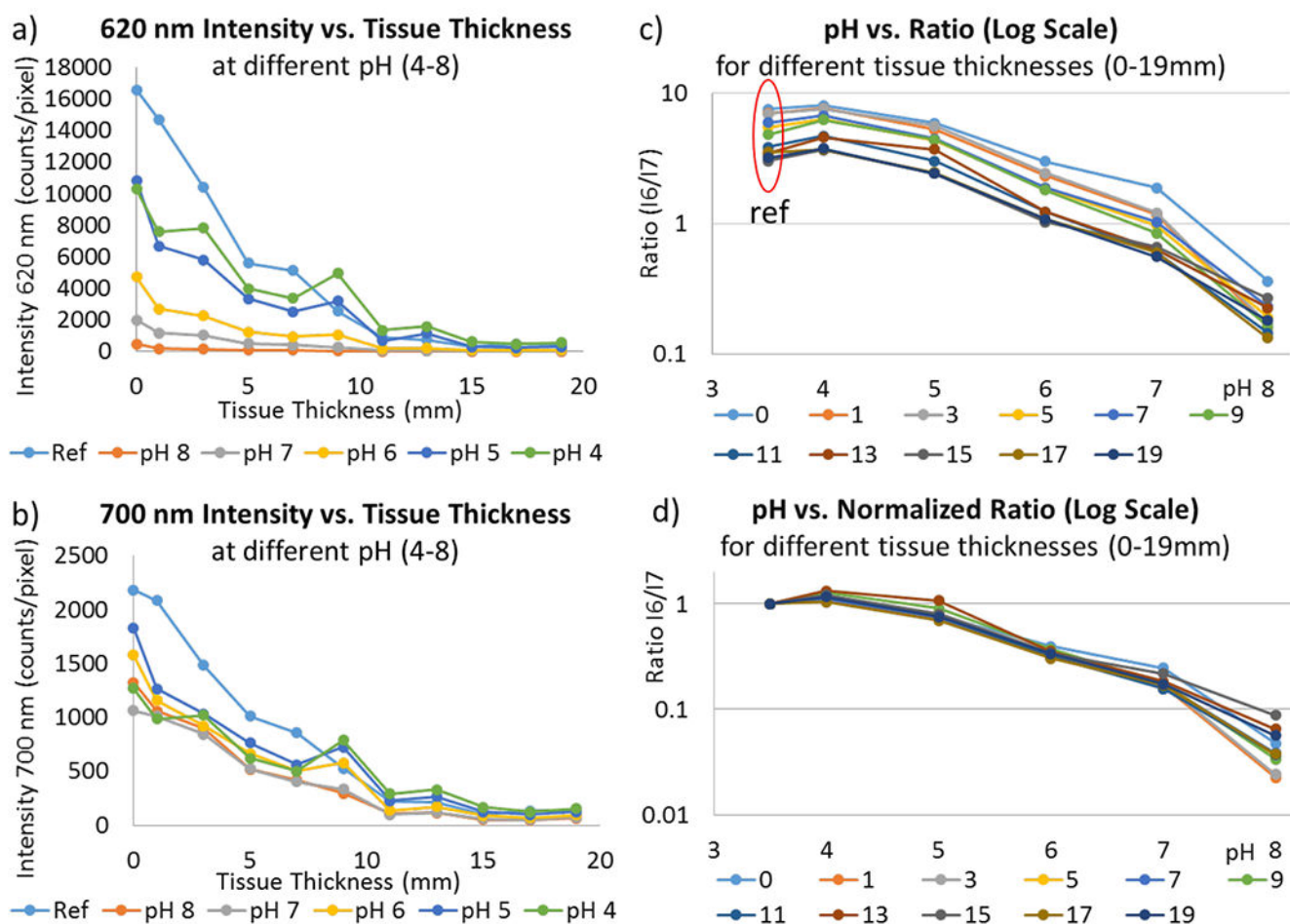
Figure 4.
Effect of tissue thickness on signal intensity. (a) 620 nm light intensity vs. tissue thickness (0 – 19 mm) at pH 4, 5, 6, 7, 8 and uncoated reference. (b) 700 nm light intensity vs. tissue thickness (0 – 19 mm) at pH 4, 5, 6, 7, 8, and uncoated reference. (c) Ratio of 620 and 700 nm intensities for each tissue thickness (0 – 19 mm) at pH 4, 5, 6, 7 and 8. Note y-axis log scale. Reference was plotted at pH 3.5. (d) Plot (c) normalized to reference value. All tissue intensities (0 – 19 mm) show good overlap at different pH except for pH 8 due to relatively weak signal intensity and higher signal to noise ratio at pH 8. Note y-axis log scale.
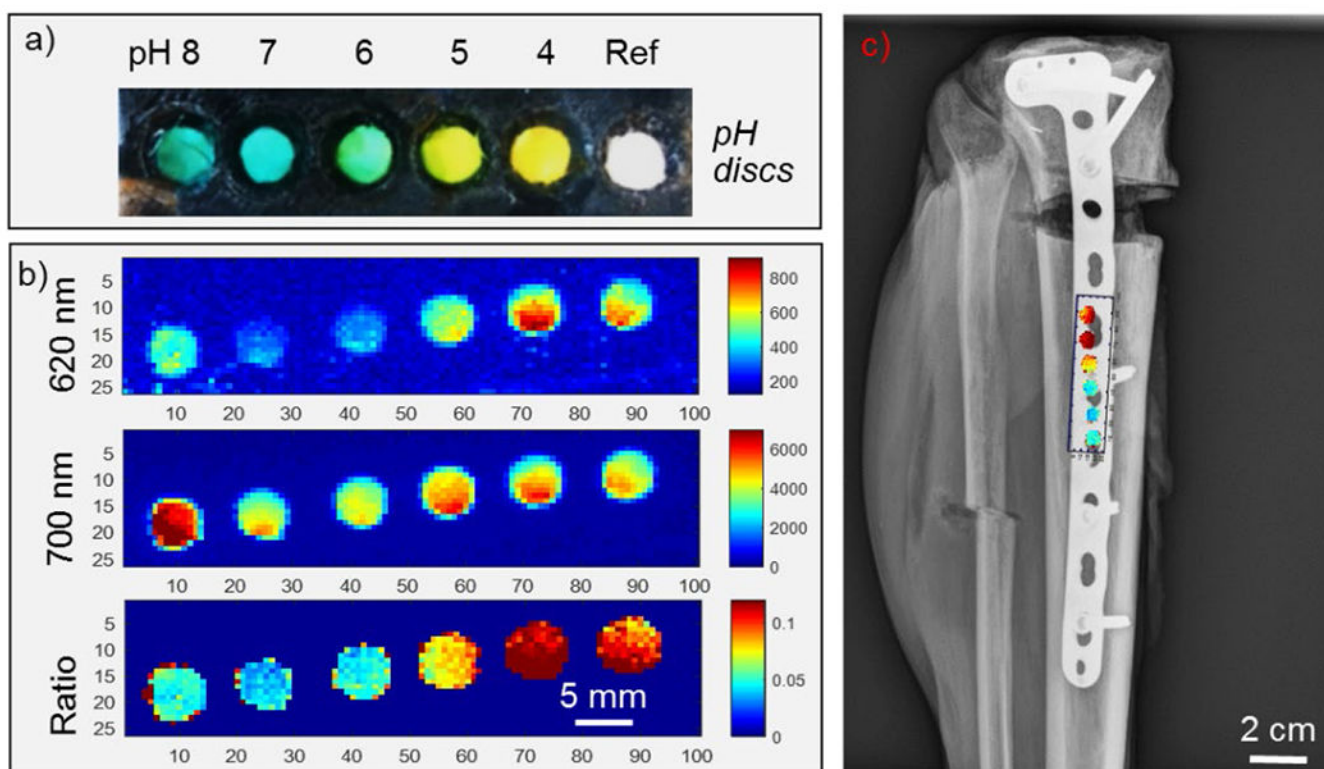
Figure 5.
Imaging pH sensor discs fixed on a tibial plate on a cadaveric specimen. (a) Photograph of pH sensor discs (5 mm in diameter) placed in a 3-D printed clip in pH buffers (left to right) 8, 7, 6, 5, 4, and a reference disc without any pH coating. (b) XELCI images of the pH sensor clip fixed on the tibial plate: Top image: 620 nm light intensity; middle image: 700 nm light intensity; bottom image: Ratio of 620/700 nm intensities. (c) X-ray radiograph of the human cadaveric tibia superimposed with XELCI image of the pH sensor discs.
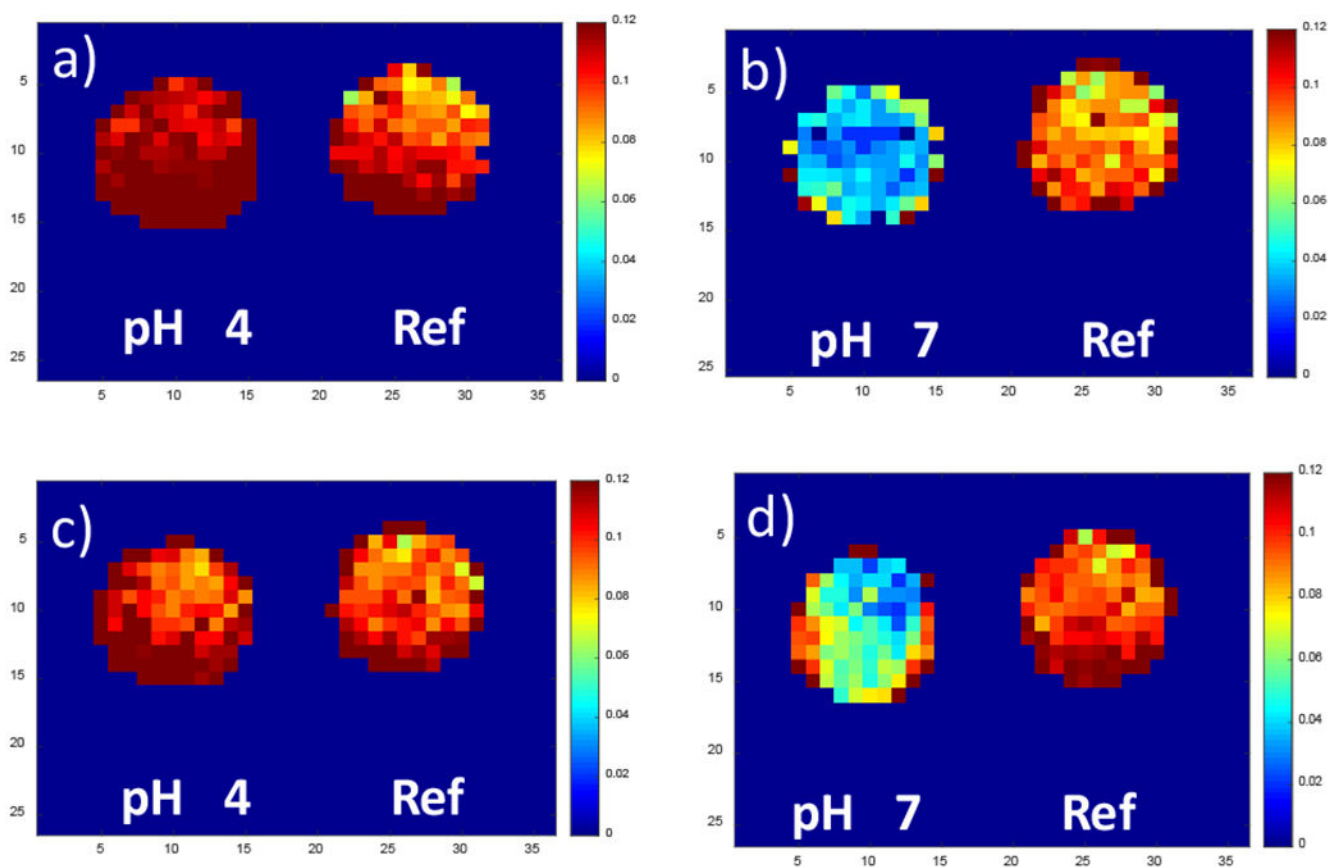
Figure 6.
pH reversibility through cadaveric tissue. XELCI ratiometric images (I700/I620 nm) of the pH sensor clip with two wells fixed on a tibial plate through human cadaveric tissue. Right well contained only the reference scintillator film and the left well had the pH sensing gel film on top of the scintillator layer. The pH of the left well was cycled between 4 and 7 by rinsing with pH 4 and pH 7 buffers alternatively followed by imaging with XELCI through tissue. (a) and (c), set to pH 4. (b) and (d), set to pH 7.